Journal of Power Sources 196 (2011) 7828–7834

Contents lists available at ScienceDirect

Journal of Power Sources

journal homepage: www.elsevier.com/locate/jpowsour

Improved pseudocapacitive performance and cycle life of cobalt hydroxide on an electrochemically derived nano-porous Ni framework

Chih-Ming Wu [a], Chen-Yen Fan [b], I-Wen Sun [a], Wen-Ta Tsai [c], Jeng-Kuei Chang [b,*]

[a] Department of Chemistry, National Cheng Kung University, 1 University Road, Tainan City, Taiwan
[b] Institute of Materials Science and Engineering, National Central University, 300 Jhongda Road, Taoyuan County, Taiwan
[c] Department of Materials Science and Engineering, National Cheng Kung University, 1 University Road, Tainan City, Taiwan

ARTICLE INFO

Article history:
Received 12 October 2010
Received in revised form 9 March 2011
Accepted 29 March 2011
Available online 5 April 2011

Keywords:
Supercapacitor
Cobalt hydroxide
Nano-porous electrode
Energy storage
Cyclic stability

ABSTRACT

The pseudocapacitance and morphology of an electrodeposited cobalt hydroxide ($Co(OH)_2$) significantly depends on the architecture of the electrode substrate. The nano-porous Ni framework, derived from the selective dissolution of Cu from a Ni–Cu alloy, effectively promotes the electrochemical utilization of deposited $Co(OH)_2$ even at a high loading amount condition. The great electronic and ionic conduction within the nano-structured electrode improves the energy storage performance of $Co(OH)_2$ as compared to that for a conventional flat Ni substrate. In this work, the $Co(OH)_2$ mass specific capacitance, evaluated using cyclic voltammetry (CV), only slightly decreases from 2650 to 2470 F g^{-1} when the potential sweep rate is substantially increased from 5 to 200 mV s^{-1}. The developed $Ni(OH)_2$/NiOOH (from the nano-porous framework) incorporates with the deposited $Co(OH)_2$ upon CV cycling; the mixed hydroxide shows a noticeably synergistic capacitance. Furthermore, the dissolution of $Co(OH)_2$ in KOH electrolyte is greatly suppressed due to the incorporation of $Ni(OH)_2$/NiOOH, consequently prolonging the electrode cycle life.

1. Introduction

Supercapacitors are energy storage devices and have recently become increasingly attractive for use in many applications, such as hybrid electric vehicles, consumer electronics, medical devices, and military missile systems, due to their greater power density and longer cycle life compared to those of batteries as well as their higher energy density compared to that of conventional capacitors [1]. Pseudocapacitors, whose capacitance is mainly attributed to the continuous and reversible redox reaction of electrode materials [2,3], are one kind of supercapacitor. $Co(OH)_2$, which has high electrochemical activity and great reversibility [4–6], is one of the most promising alternatives (among MnO_x, CoO_x, NiO_x, and FeO_x) to traditional RuO_2 electrodes [7] in pseudocapacitors, since the high cost of the latter has limited its commercial usage. Despite its importance, research on the pseudocapacitive properties of $Co(OH)_2$ has been limited. Further improvement in its energy density and power density are desired. Moreover, the effects of the $Co(OH)_2$ loading amount (on a current collector) on the charge storage performance should be clarified before the electrodes can be used in practice.

Nanomaterials with a feature size ranging from a few to hundreds of nanometers have great potential for electrochemical energy storage applications [1,8]. In a nano-structured electrode, the distance within the material over which electrolyte ions must be transported is shorter than that within a bulk electrode. Furthermore, a large surface area allows for a high current (or reaction rate) during the redox transition. As a result, superior charge storage/delivery performance can be obtained as compared to that of a conventional bulk electrode [9,10]. Construction of nano-architectured electrodes for supercapacitor applications has been attempted in previous studies [11–14]. Self-supported oxide nanotubes or nanorods [15–17] and carbon-supported (e.g., using CNTs or activated carbon) oxide nano-particles [18–20] have been fabricated. Recently, we proposed an approach that uses nano-porous Ni frameworks as substrates (or current collectors) [21] for loading the electro-active materials (e.g., MnO_2 and Co_3O_4) to obtain nano-structured electrodes [22,23]. Considerable improvement in the pseudocapacitive performance was confirmed (as compared to that obtained using a conventional flat substrate). The high-porosity Ni was developed from the selective dissolution of Cu from an electrodeposited Ni–Cu layer; then, the metal oxides were electrodeposited. Therefore, the preparation of nano-structured electrodes is an entirely electrochemical process, which has the advantages of simplicity, reliability, accuracy, versatility, and low-cost [24,25]. Moreover, the nano-structure is self-supported and binder-less and is characterized by its concave geometry. The proposed protocol can be generally performed on any conductive surface, which can be inexpensive, lightweight, flexible, and wear-

* Corresponding author. Tel.: +886 3 422 7151x34908; fax: +886 3 280 5034.
E-mail address: jkchang@ncu.edu.tw (J.-K. Chang).

0378-7753/$ – see front matter © 2011 Elsevier B.V. All rights reserved.
doi:10.1016/j.jpowsour.2011.03.083

able, allowing the prepared supercapacitors to be integrated into mobile micro-power systems.

In the present study, $Co(OH)_2$ is cathodically deposited on nano-porous Ni frameworks; the effects of loading on the supercapacitor properties are studied for the first time. The electrochemical utilization of the active material (with various thicknesses) on flat and nano-porous substrates is systematically examined at various charge–discharge rates. In practice, a higher loading of the active material with great utilization (especially under a high-power condition) is desired, since it leads to superior charge storage performance of the electrode. Additionally, the prepared nano-structured electrode exhibits an excellent cycle life. The detailed mechanism is proposed and discussed.

2. Experimental

A Ni–Cu alloy layer was electrodeposited from a plating solution containing 1 M $NiSO_4$, 0.01 M $CuSO_4$, and 0.5 M H_3BO_3 (pH = 4). This procedure was performed at 25 °C in a three-electrode cell with a platinum counter electrode and a saturated calomel reference electrode (SCE). Ni foil with an exposed area of 1 cm^2 was used as the working electrode (i.e., the substrate). The alloy was deposited under a constant potential of −0.75 V, and the total cathodic charge was set at 3 C cm^{-2}. Selective anodic dissolution of Cu from the obtained Ni–Cu film was then conducted in the same solution by changing the applied potential to +0.2 V. Afterward, $Co(OH)_2$ was cathodically deposited onto the developed nano-porous Ni framework and flat Ni foil, respectively, in 0.1 M $Co(CH_3COO)_2$ aqueous solution at 25 °C. The electrochemical cell employed was the same as that used for Ni–Cu deposition. A potential of–0.75 V was applied to yield a passed charge that ranged from 25 to 200 mC cm^{-2}. The amounts of Co deposited were quantified using an atomic absorption spectrometer (AAS, SOLAAR M6); in these analyses, the deposits were totally dissolved in 0.1 M HNO_3 solution before measurements.

Surface morphologies and chemical compositions of the samples were examined using a scanning electron microscope (SEM, Philip XL-40 FEG) and its auxiliary X-ray energy dispersive spectrometer (EDS). An Auger electron spectrometer (AES, Thermo Microlab 350) was employed to locally probe the surface chemistry. The typical analysis diameter was ~20 nm. The crystal structure of the deposit was explored using a glancing angle X-ray diffractometer (GAXRD, Rigaku D/MAX 2500), which is more surface sensitive than traditional XRD.

The pseudocapacitive properties of various $Co(OH)_2$ electrodes were studied using cyclic voltammetry (CV) in 1 M KOH solution at 25 °C. The potential was scanned in a range of −0.2 to 0.45 V with sweep rates ranging from 5 to 200 mV s^{-1}. At least five parallel samples prepared under identical conditions were tested; the deviation of the measured capacitances was typically within 5%. The data reported in this paper are the medians. CV multi-scans with a sweep rate of 50 mV s^{-1} were performed for up to 4000 cycles to evaluate the cyclic stability of the electrodes. After the test, AAS was used to measure the remaining amounts of $Co(OH)_2$ on the substrates. X-ray photoelectron spectroscopy (XPS) was employed to study the chemical state variation upon cycling; the analyses were performed with a PHI 5000 Versa-Probe spectrometer utilizing monochromated Al Kα radiation as the X-ray source.

3. Results and discussion

The SEM micrograph in Fig. 1(a) shows the surface morphology of the electrodeposited Ni–Cu alloy. During the electrodeposition, new grains (~100 nm in diameter) formed on previous ones (i.e., progressive nucleation), growing into a protruding structure. The

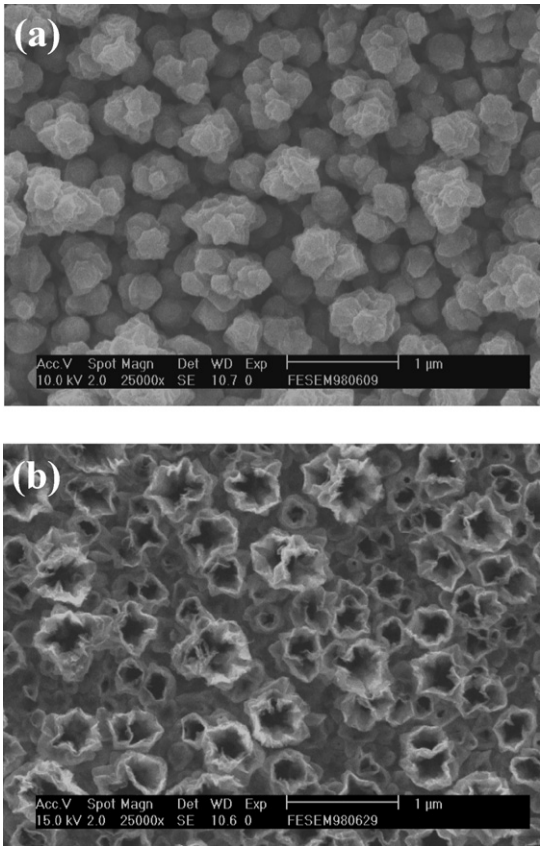

Fig. 1. (a) SEM micrograph of the electrodeposited Ni–Cu film. (b) Porous structure developed from the formation in (a) after the electrode was etched at +0.2 V.

AES analytical results indicated that the central part of each grain was a Cu-rich domain with a Ni/Cu/O atomic ratio of approximately 10/70/20 whereas the surrounding Ni-rich area had a composition ratio of about 70/10/20. The detected oxygen was attributed to the partial oxidation of the electrode surface upon exposure to air or the adsorbed water on the sample or both. The observed nano-scale chemical segregation is in good agreement with that found in a TEM study reported by Searson and co-workers [26]. Fig. 1(b) shows the porous structure that developed from the deposit shown in Fig. 1(a) (after +0.2 V anodic etching). The AES data indicated that the remaining framework had a surface Ni/Cu/O atomic ratio of 53/2/45, confirming that most of the Cu was selectively extracted from the deposit. Of note, the oxygen concentration is much higher than those found on the as-deposited alloy film. This oxygen cannot be detected by EDS, which typically has an analytical depth of a few microns. AES and EDS data suggest that a surface passivation layer (a nanometer-deep oxide film) was formed on Ni, preventing it from being anodically dissolved. Cu, which was in the central part of each grain, was preferentially removed, leaving behind the Ni porous framework. It was noticed that the clustered Ni–Cu grains, formed during the deposition, led to the development of connected pores upon etching. As a result, a petal-like structure with a pore diameter of approximately 150 nm can be observed in Fig. 1(b); the pore density was found to be $\sim 10^{13}$ m^{-2}. The feature size of the obtained architecture is much smaller than those of existing commercial Ni foam and stainless steel mesh substrates used for pseudocapacitors (their pore sizes are on the micrometer scale) [27,28]. Thus, more pronounced nano-structure effects of the electrode can be expected.

With the efficient and easy electrochemical protocol for creating a Ni nano-porous framework established, the electrodeposition of

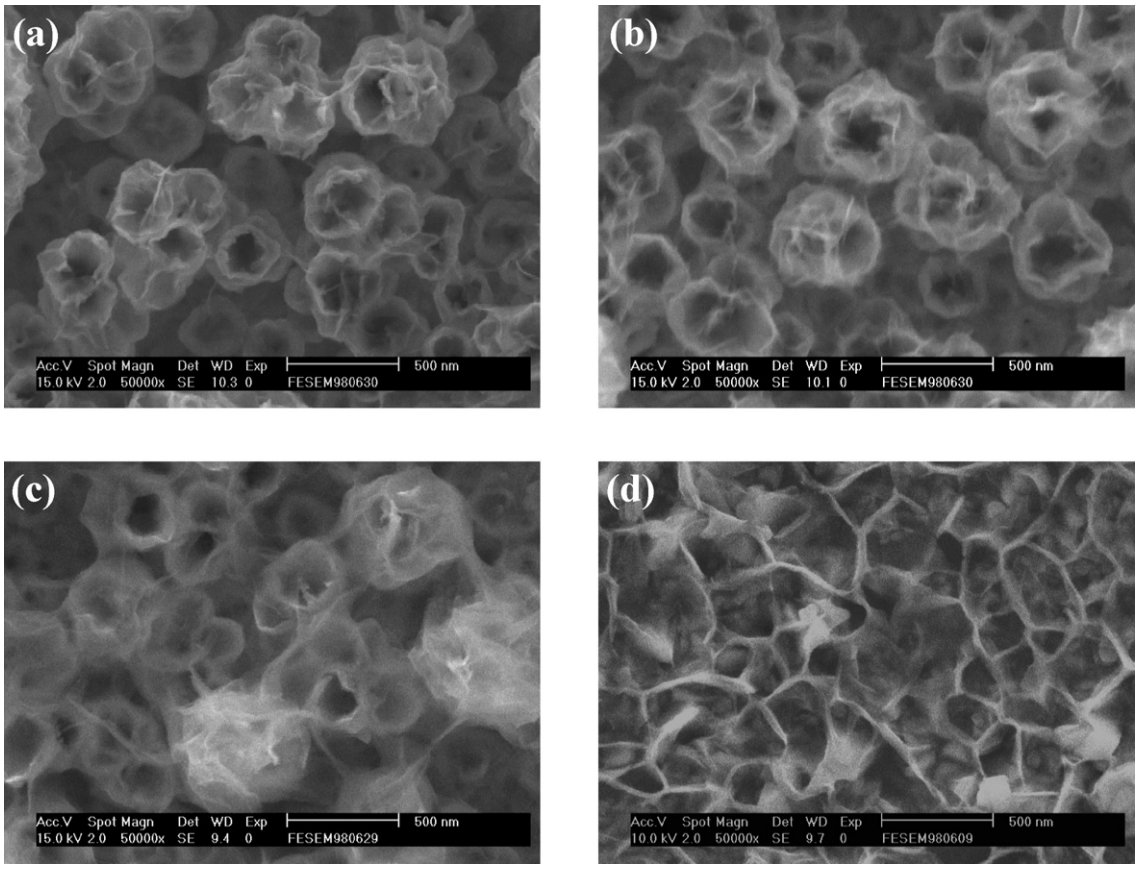

Fig. 2. SEM micrographs of the nano-structured electrodes with $Co(OH)_2$ deposition amounts of (a) 50, (b) 100, and (c) 150 mC cm^{-2}, respectively. The morphology of the 100 mC cm^{-2}-deposited $Co(OH)_2$ on a flat Ni substrate is shown in (d) for comparison.

cobalt hydroxide on this substrate was then attempted. A cathodic potential of −0.75 V was applied in 0.1 M $Co(CH_3COO)_2$ solution; Fig. 2(a)–(c) shows the SEM micrographs of the obtained nano-structured electrodes with deposition charges of 50, 100, and 150 mC cm^{-2}, respectively. As demonstrated, the high-porosity Ni framework provided a large surface area for dispersing the deposit. With increasing deposition charge, the amount of deposit gradually increased; however, silk-like deposits with a width of just a few nanometers were uniformly distributed on the nano-size Ni petals, even when the deposition amount was tripled. Fig. 2(d) shows a typical morphology of the deposit on a flat Ni substrate (with a deposition charge of 100 mC cm^{-2}). Much thicker ribbons with entanglement were observed above a granular but compact lower layer. The experimental results clearly indicate that the electrode substrate plays a significant role in the morphology of the deposit. When the nano-architectured Ni was used, well-dispersed $Co(OH)_2$ nano-silk was obtained. It was found that the deposition current density on the nano-porous Ni is approximately 30 times higher than that on a flat Ni substrate, suggesting that the true electrochemical surface area of the former electrode is ∼30-fold the apparent area.

The crystal structure of the deposit was examined using GAXRD; a typical diffraction pattern is shown in Fig. 3. Besides the two strong signals associated with the Ni substrate, the peaks located at 19.0° and 37.8° were respectively identified to be the (0 0 1) and (1 0 1) diffractions of $Co(OH)_2$, which has a hexagonal structure (JCPDS No. 73-6993). However, the broad peaks with low diffraction intensity suggest that the deposited $Co(OH)_2$ is nano-crystalline. This result is consistent with SEM observations.

The amount of $Co(OH)_2$ loading on the nano-porous Ni framework was quantified using AAS. Fig. 4 shows the mass of $Co(OH)_2$ as a function of the cathodic deposition charge. A linear relationship with a regression slope of 0.479 μg mC^{-1} was found, which is quite close to the theoretical value of 0.481 μg mC^{-1} for a two-charge-transfer deposition reaction of $Co(OH)_2$. Accordingly, the following electrodeposition mechanism is proposed (also taking into account the applied potential of −0.75 V, which can decompose water):

$$H_2O + 2e^- \rightarrow H_2 + 2OH^- \quad (1)$$

$$Co^{2+} + 2OH^- \rightarrow Co(OH)_2 \quad (2)$$

The same $Co(OH)_2$ mass-to-charge relationship (as in Fig. 4) was found for a flat Ni electrode, indicating an identical deposition course regardless of the substrate. It can be concluded that the

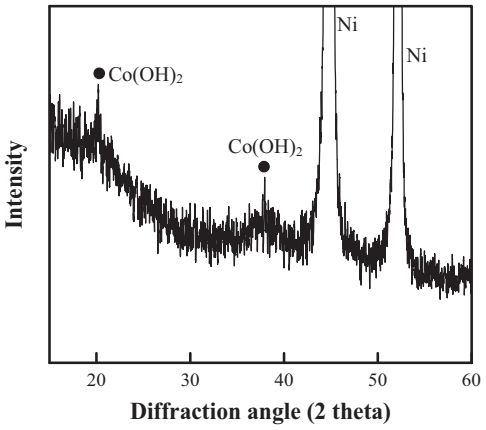

Fig. 3. GAXRD pattern of the prepared nano-structured electrode.

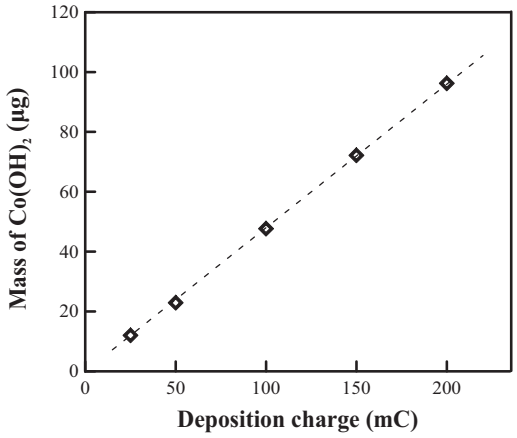

Fig. 4. Mass of $Co(OH)_2$ evaluated using an atomic absorption spectrometer (AAS) as a function of cathodic deposition charge.

loading of $Co(OH)_2$ can be easily controlled by regulating the total cathodic charge applied.

After the nano-structured $Co(OH)_2$ electrodes (with porous Ni framewok) were constructed via an entirely electrochemical process, their pseudocapacitive characteristics were evaluated. Curves *a*–*c* in Fig. 5(a) are the cyclic voltammograms of the electrodes with $Co(OH)_2$ deposition amounts of 50, 100, and 150 mC cm^{-2}, respectively, recorded in 1 M KOH solution with a potential sweep rate of 5 mV s^{-1}. For each curve, two symmetric anodic/cathodic pairs superimposed on a broad redox background were obtained, indicating satisfactory pseudocapacitive performance of the $Co(OH)_2$ electrode. According to the literature [12,27], the observed two reversible redox couples (a_1/c_1 at ~0.02 V; a_2/c_2 at ~0.26 V) can be expressed as:

$$Co(OH)_2 + OH^- \leftrightarrow CoOOH + H_2O + e^- \quad (3)$$

$$CoOOH + OH^- \leftrightarrow CoO_2 + H_2O + e^- \quad (4)$$

In Fig. 5(a), the CV enclosed area, which corresponds to the energy storage capability, clearly increases with increasing the $Co(OH)_2$ amount. This indicates that the bulk $Co(OH)_2$, instead of the outermost region, participates in the electrochemical reaction. The area specific capacitance (C_a) of the electrode can be evaluated according to:

$$C_a = \frac{Q}{\Delta V} \quad (5)$$

where Q is the voltammetric charge (per unit electrode area) integrated from both the positive and negative CV sweeps, and ΔV is the potential scanning extent (i.e., 0.65 V × 2). As shown in the upper plot of Fig. 5(b), the capacitance substantially increased from 60 to 120 mF cm^{-2} when the deposition charge was increased from 50 to 150 mC cm^{-2}, although a slight decline in the increasing slope was found at a higher $Co(OH)_2$ loading. Curve *d* of Fig. 5(a) shows that the electrode with a flat Ni substrate had a much smaller current response as compared to curve *a*, despite having the same $Co(OH)_2$ deposition amount (50 mC cm^{-2}). The area specific capacitance was only about 12 mF cm^{-2}, indicating a noticeably inferior charge storage capacity of the deposited $Co(OH)_2$. Moreover, as depicted in the lower plot in Fig. 5(b), the measured capacitance does not considerably increase with $Co(OH)_2$ deposition charge. This result implies that only the surface portion of the hydroxide was involved in the pseudocapacitive reaction; the underlying layer could not be accessed (or utilized) due to its relatively compact structure (as demonstrated in Fig. 2). Clearly, the nano-porous substrate is more suitable for loading a higher quantity of electroactive material, benefiting the area specific capacitance.

The mass specific capacitance (C_m) of the electrodes can also be quantitated based on the weights of $Co(OH)_2$. The calculated C_m values for the 50 mC-deposited $Co(OH)_2$ on flat and nano-porous Ni substrates were 550 and 2650 F g^{-1}, respectively. While the former is close to previously reported data [6,28–30], the latter is among the best values achieved so far [12,27]. The high surface area of the nano-structured electrode significantly extended the electro-active sites for the pseudocapacitive reaction. Moreover, the high-porosity architecture enhanced the electrolyte accessibility and thereby led to superior electrode reactivity. As a result, the nano-structured $Co(OH)_2$ electrode exhibited much better charge storage performance as compared to that of the traditional version of the electrode. According to Eqs. (3) and (4), the theoretical capacitance of $Co(OH)_2$ over a potential window of 0.65 V is 3195 F g^{-1}. A capacitance utilization of as high as 83% was achieved on the nano-porous Ni substrate due to the high dispersion of the nano-size $Co(OH)_2$ (Fig. 2); this ratio is approximately 4.8 times higher than that (~17%) of the conventional $Co(OH)_2$ counterpart. When the $Co(OH)_2$ deposition was increased to 150 mC cm^{-2}, the C_m values were lowered to 1665 F g^{-1} (on nano-porous Ni) and 225 F g^{-1} (on flat Ni), respectively. The utilization improvement due to the use of the unique Ni framework was even more pronounced (7.4 times vs. 4.8 times) when a higher quantity of $Co(OH)_2$ was loaded. High utilization also implies the possibility of reducing the amount of active material used (and thus the cost of the electrode), preserving natural resources.

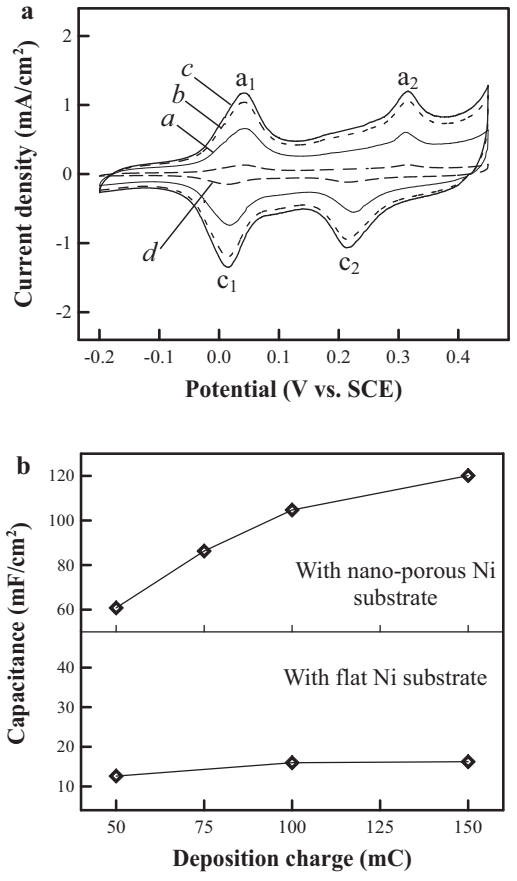

Fig. 5. (a) Cyclic voltammograms of the nano-structured electrodes with $Co(OH)_2$ deposition amounts of 50 (curve *a*), 100 (curve *b*), and 150 mC cm^{-2} (curve *c*), recorded in 1 M KOH solution with a potential sweep rate of 5 mV s^{-1}. The voltammogram of the 50 mC cm^{-2}-deposited $Co(OH)_2$ electrode with a flat Ni substrate is shown in curve *d* for comparison. (b) Area specific capacitances as a function of $Co(OH)_2$ deposition charge on nano-porous and flat Ni substrates.

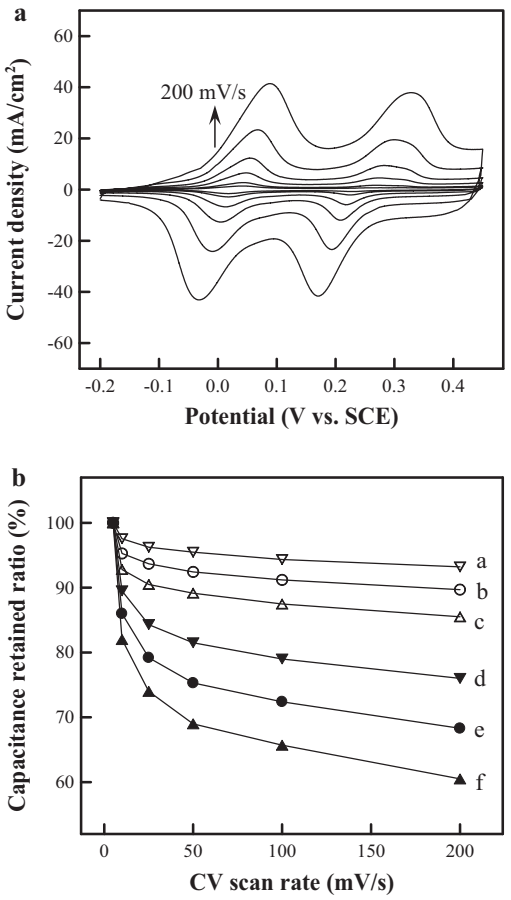

Fig. 6. (a) Cyclic voltammograms of the nano-structured electrode with a $Co(OH)_2$ deposition amount of 100 mC cm^{-2} measured at potential sweep rates of 5, 10, 25, 50, 100, and 200 mV s^{-1}. (b) Capacitance retained ratios as a function of the CV scan rate for nano-structured electrodes (curves *a*–*c*) and conventional flat-substrate electrodes (curves *d*–*f*). The $Co(OH)_2$ deposition amounts were 50 mC cm^{-2} (curves *a*, *d*), 100 mC cm^{-2} (curves *b*, *e*), and 150 mC cm^{-2} (curves *c*, *f*).

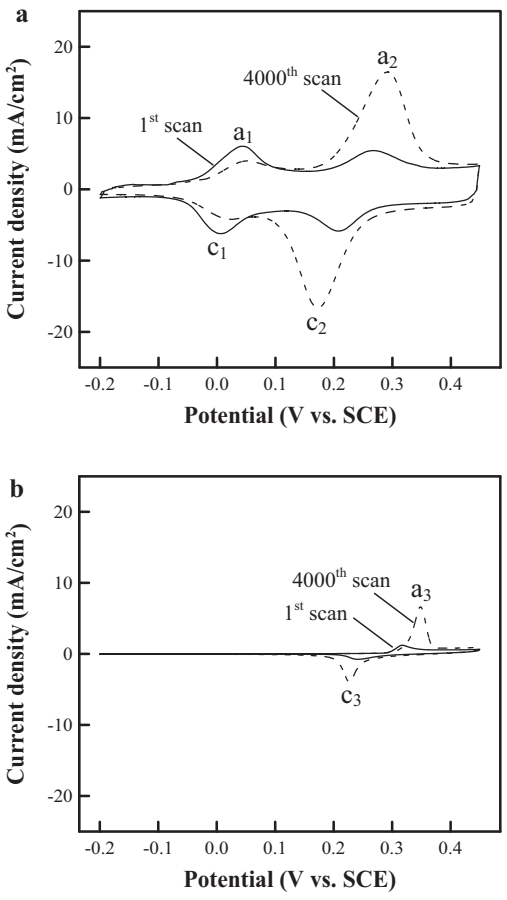

Fig. 7. Initial and the 4000th CV scans of (a) the nano-structured electrode with a $Co(OH)_2$ deposition amount of 50 mC cm^{-2} and (b) a bare porous Ni substrate measured in 1 M KOH electrolyte with a potential sweep rate of 50 mV s^{-1}.

Fig. 6(a) shows the CV curves of a typical nano-structured electrode, which has a $Co(OH)_2$ deposition amount of 100 mC cm^{-2}, measured at various potential sweep rates. The mirror-image characteristics (with symmetric anodic and cathodic peaks) can be maintained even at a high CV rate of 200 mV s^{-1}. Moreover, the response current of the electrode increased almost linearly with increasing potential scan rate. These results show the excellent kinetic performance and reversibility of the nano-structured electrode. Fig. 6(b) demonstrates the capacitance retained ratios as a function of CV scan rate for various electrodes prepared in this study. Clearly, the nano-structured electrodes show superior high-rate performance as compared to that of traditional electrodes. For example, with a $Co(OH)_2$ deposition amount of 50 mC cm^{-2}, the electrode using the nano-porous Ni substrate retained over 93% capacitance when the potential scan rate was increased from 5 to 200 mV s^{-1} whereas the flat counterpart electrode retained only 76% capacitance under the same condition. When the $Co(OH)_2$ loading was increased to 150 mC cm^{-2}, a satisfactory capacitance retained ratio of 86% can still be achieved for the nano-structured electrode (when the CV scan rate raised from 5 to 200 mV s^{-1}); however, a much lower value of 60% was found for the flat electrode due to its kinetic limitation. The superior high-rate performance of the nano-structured electrode can be attributed to three major factors: (i) the high porosity increases OH^- transport, promoting ionic conduction within the electrode (ii) the greatly dispersed $Co(OH)_2$ shortens the electron travelling distance, improving the electronic conduction, and (iii) the high contact area between the substrate and the electro-active material minimizes the interface

Table 1
Mass specific capacitances (F/g) of $Co(OH)_2$ with various deposition amounts on nano-porous and flat Ni substrates. The capacitances evaluated at various CV scan rates are given.

CV scan rate	Nano-porous Ni substrate			Flat Ni substrate		
	Co(OH)2 deposition amount					
	50 mC cm^{-2}	100 mC cm^{-2}	150 mC cm^{-2}	50 mC cm^{-2}	100 mC cm^{-2}	150 mC cm^{-2}
5 mV s^{-1}	2650	2210	1665	550	335	225
10 mV s^{-1}	2585	2105	1545	492	288	185
25 mV s^{-1}	2550	2070	1505	464	265	167
50 mV s^{-1}	2530	2045	1485	448	252	155
100 mV s^{-1}	2500	2015	1455	435	243	148
200 mV s^{-1}	2470	1980	1425	418	229	136

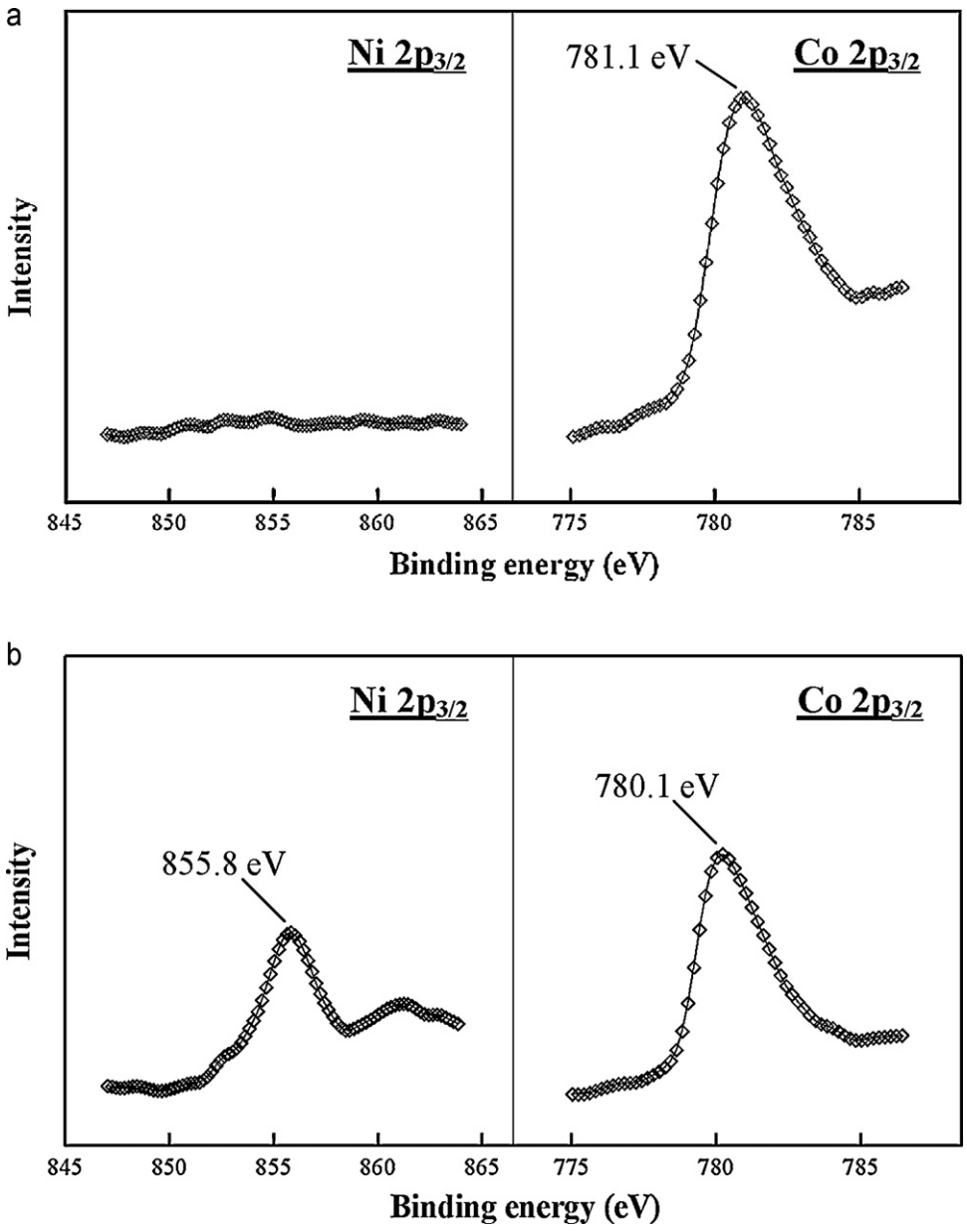

Fig. 8. XPS Ni $2p_{3/2}$ and Co $2p_{3/2}$ spectra taken from the nano-structured electrode with a $Co(OH)_2$ deposition amount of 50 mC cm^{-2} (a) before and (b) after 4000 CV scans.

resistance, facilitating charge transfer reactions. The mass specific capacitances of various electrodes at different CV scan rates are summarized in Table 1. It should be noted that the capacitances of the nano-structured electrodes at a high-rate condition outperform the existing $Co(OH)_2$ electrodes reported in the literature [4,6,27,28,31]. This result indicates the great advantage of using the proposed strategy to construct supercapacitor nano-structured electrodes, since their high-power performance is particular concern.

Redox cyclic stability (i.e., cycle life) of electrodes is an important concern in supercapacitors. A gradual capacitance decay of $Co(OH)_2$ with charge–discharge cycling has been reported in the literature [6,12,28–31]. With a flat Ni substrate, a 25% capacitance decay was detected in this study after 500 CV cycles, which is in good agreement with previously reported data [6,29,30]. AAS analytical data revealed that only ~75% of the initial $Co(OH)_2$ remained after cycling, indicating that the capacitance fading mainly resulted from the dissolution of the active material. Interestingly, it was found that the measured capacitance of the nano-structured electrode did not deteriorate upon cycling. Fig. 7(a) shows the initial and the 4000th CV curves of the 50 mC-deposited $Co(OH)_2$ electrode with the porous Ni substrate. While the a_1/c_1 redox couple gradually weakened, the a_2/c_2 intensity clearly became stronger. After 4000 CV cycles, the electrochemical response reached a steady state; as illustrated in Fig. 7(a), an approximately 50% voltammetric charge increase was obtained. In order to clarify where the extra charge came from, a bare porous Ni electrode was subjected to the same CV test (4000 cycles); the results are shown in Fig. 7(b). The a_3/c_3 redox couple located at ~0.3 V can be attributed to the following reaction [32,33]:

$$Ni(OH)_2 + OH^- \leftrightarrow NiOOH + H_2O + e^- \quad (6)$$

It is noted that the Ni electrode reacted with the alkaline electrolyte to form $Ni(OH)_2$. While the a_3/c_3 current was negligible in the initial cycle, it gradually increased to become saturated after ~4000 cycles. The high surface area facilitated a considerable amount of $Ni(OH)_2$ species to develop over the porous electrode when it contacted the electrolyte, leading to the apparent a_3/c_3

increase. The increase in current was retarded (with cycling) after the electrode surface was covered by a massive $Ni(OH)_2$ layer, because further evolution of the new hydroxide by a diffusion process became more difficult. However, comparing the peak position and the current variation upon cycling in Fig. 7(a) and (b), it is concluded that the capacitance increase of the nano-structured $Co(OH)_2$ electrode cannot be exclusively ascribed to the contribution from $Ni(OH)_2$/NiOOH (even if the porous substrate is fully accessible to the electrolyte). The incorporation of $Ni(OH)_2$/NiOOH into the deposited $Co(OH)_2$, probably forming a Co–Ni mixed hydroxide, is speculated to contribute to the synergistic enhancement in the a_2/c_2 intensity shown in Fig. 7(a). Since the mixed hydroxide may not be reduced to $Co(OH)_2$ (as in Eq. (3)), the a_1/c_1 couple in Fig. 7(a) diminished. The high-porosity architecture of the electrode (thus large substrate/deposit contact interface and high electrolyte accessibility) assisted the incorporation of the oxidized Ni with the $Co(OH)_2$ nano-silk (as shown in Fig. 2(a)–(c)), thus leading to the formation of the mixed hydroxide, which barely developed when the Ni plate was shielded by a compact $Co(OH)_2$ layer (Fig. 2(d)). The a_2/c_2 couple at the 4000th cycle (Fig. 7(a)) can be deconvoluted into three constituents including $Co(OH)_2$, Co–Ni mixed hydroxide, and $Ni(OH)_2$; the calculated peak area ratios are approximately 35%, 55%, and 10%, respectively (assuming the $Co(OH)_2$ and $Ni(OH)_2$ peak position and shape are similar to those found when they exist individually). This suggests that the measured ~50% voltammetric charge increase after cycling mainly came from the redox reaction of the newly developed Co–Ni mixture. The testing electrolyte used for Fig. 7(a) after 4000 CV cycles was also analyzed using AAS; the data revealed that negligible Co and Ni concentrations were detected. This result implies that the dissolution of $Co(OH)_2$ in the KOH solution upon cycling was significantly suppressed due to the consolidation with $Ni(OH)_2$/NiOOH.

The chemical state variation of the nano-structured electrode upon charge–discharge cycling was further examined using XPS. Fig. 8(a) shows the Ni $2p_{3/2}$ and Co $2p_{3/2}$ spectra of the as-prepared electrode (before cycling). Little Ni signal was found on the electrode, confirming that the surface was predominantly covered by the deposit. The Co peak located at 781.1 eV can be attributed to $Co(OH)_2$ [34], which is consistent with the GAXRD result in Fig. 3. After 4000 CV scan cycles, as shown in Fig. 8(b), a clear Ni peak appeared, verifying the diffusion of Ni towards the electrode surface. It should be mentioned that the CV multi-scans ended at −0.2 V. The measured binding energy peak at 855.8 eV confirms the existence of $Ni(OH)_2$ on the electrode [35]; this result is in agreement with Eq. (6) since a more reduced species was anticipated at the low termination potential. Due to the incorporation of $Ni(OH)_2$, the intensity of the Co spectrum was lower than that shown in Fig. 8(a). Fig. 8(b) also shows that the Co peak shifted to the position of 780.1 eV, corresponding to CoOOH [36]. As mentioned previously (and shown in Fig. 7(a)), due to the formation of the mixed Co–Ni species, the deposited $Co(OH)_2$ cannot be fully recovered after being anodized. As a result, Co oxyhydroxide became the major phase in the electrode that underwent the repeating redox cycles.

4. Conclusion

Silk-like $Co(OH)_2$ was highly dispersed on the nano-porous Ni framework, which was easily developed from the anodic etching of Cu in an electrodeposited Ni–Cu layer. Moreover, the amount of $Co(OH)_2$ deposited can be precisely controlled by adjusting the cathodic charge. Due to the unique architecture, much higher pseudocapacitance and better high-rate redox capability were obtained (even with a high $Co(OH)_2$ loading) as compared to those of the conventional version of a flat electrode. The high-surface-area substrate facilitated the development of $Ni(OH)_2$/NiOOH, which incorporated with the deposited $Co(OH)_2$ to form a binary hydroxide upon CV cycling in KOH electrolyte. The synergistic electro-activity of the Co–Ni mixed hydroxide, which increased charge storage capacity, was confirmed. The incorporation of $Ni(OH)_2$/NiOOH also significantly inhibited the dissolution of $Co(OH)_2$ into the electrolyte, suppressing electrode deterioration during charging/discharging. The formation of the mixed hydroxide, developed from the interaction between the nano-structured deposit and the high-porosity substrate, has proposed a new concept to achieve exceptional performance of a supercapacitor electrode.

Acknowledgment

The financial support of this work by the National Science Council of the Republic of China under grants NSC 98-ET-E-006-009-ET and NSC 99-2218-E-008-007-MY3 is gratefully appreciated.

References

[1] P. Simon, Y. Gogotsi, Nat. Mater. 7 (2008) 845.
[2] K.W. Nam, M.G. Kim, K.B. Kim, J. Phys. Chem. C 111 (2007) 749.
[3] J.K. Chang, M.T. Lee, W.T. Tsai, J. Power Sources 166 (2007) 590.
[4] V. Gupta, T. Kusahara, H. Toyama, S. Gupta, N. Miura, Electrochem. Commun. 9 (2007) 2315.
[5] H.J. Ahn, W.B. Kim, T.Y. Seong, Electrochem. Commun. 10 (2008) 1284.
[6] P.K. Nayak, N. Munichandraiah, J. Electrochem. Soc. 155 (2008) A855.
[7] J.P. Zheng, P.J. Cygan, T.R. Jow, J. Electrochem. Soc. 142 (1995) 2699.
[8] Z.L. Wang, Adv. Mater. 15 (2003) 1497.
[9] R.H. Baughman, A.A. Zakhidov, W.A. de Heer, Science 297 (2002) 787.
[10] A.S. Aricò, P. Bruce, B. Scrosati, J.M. Tarascon, W. van Schalkwijk, Nat. Mater. 4 (2005) 366.
[11] W. Sugimoto, H. Iwata, Y. Yasunaga, Y. Murakami, Y. Takasu, Angew. Chem. Int. Ed. 42 (2003) 4092.
[12] L. Cao, F. Xu, Y.Y. Liang, H.L. Li, Adv. Mater. 16 (2004) 1853.
[13] D. Choi, G.E. Blomgren, P.N. Kumta, Adv. Mater. 18 (2006) 1178.
[14] J.K. Chang, C.H. Huang, W.T. Tsai, M.J. Deng, I.W. Sun, J. Power Sources 179 (2008) 435.
[15] C.C. Hu, K.H. Chang, M.C. Lin, Y.T. Wu, Nano Lett. 6 (2006) 2690.
[16] Y. Wang, K. Takahashi, K.H. Lee, G.Z. Cao, Adv. Funct. Mater. 16 (2006) 1133.
[17] R. Liu, S.B. Lee, J. Am. Chem. Soc. 130 (2008) 2942.
[18] A.E. Fischer, K.A. Pettigrew, D.R. Rolison, R.M. Stroud, J.W. Long, Nano Lett. 7 (2007) 281.
[19] S.L. Chou, J.Z. Wang, S.Y. Chew, H.K. Liu, S.X. Dou, Electrochem. Commun. 10 (2008) 1724.
[20] K.W. Nam, C.W. Lee, X.Q. Yang, B.W. Cho, W.S. Yoon, K.B. Kim, J. Power Sources 188 (2009) 323.
[21] J.K. Chang, S.H. Hsu, I.W. Sun, W.T. Tsai, J. Phys. Chem. C 112 (2008) 1371.
[22] J.K. Chang, S.H. Hsu, W.T. Tsai, I.W. Sun, J. Power Sources 177 (2008) 676.
[23] M.J. Deng, F.L. Huang, I.W. Sun, W.T. Tsai, J.K. Chang, Nanotechnology 20 (2009) 175602.
[24] G.S. Attard, P.N. Bartlett, N.R.B. Coleman, J.M. Elliott, J.R. Owen, J.H. Wang, Science 278 (1997) 838.
[25] P.A. Nelson, J.M. Elliott, G.S. Attard, J.R. Owen, Chem. Mater. 14 (2002) 524.
[26] Z. Liu, D. Elbert, C.L. Chien, P.C. Searson, Nano Lett. 8 (2008) 2166.
[27] W.J. Zhou, M.W. Xu, D.D. Zhao, C.L. Xu, H.L. Li, Micropor. Mesopor. Mater. 117 (2009) 55.
[28] S.L. Chou, J.Z. Wang, H.K. Liu, S.X. Dou, J. Electrochem. Soc. 155 (2008) A926.
[29] C. Yuan, X. Zhang, B. Gao, J. Li, Mater. Chem. Phys. 101 (2007) 148.
[30] Z. Hu, L. Mo, X. Feng, J. Shi, Y. Wang, Y. Xie, Mater. Chem. Phys. 114 (2009) 53.
[31] W.J. Zhou, J. Zhang, T. Xue, D.D. Zhao, H.L. Li, J. Mater. Chem. 18 (2008) 905.
[32] M. Fleischmann, J. Koryta, H.R. Thrisk, Trans. Faraday Soc. 63 (1967) 1261.
[33] V. Srinivasan, J.W. Weidner, J. Electrochem. Soc. 144 (1997) L210.
[34] T.L. Barr, J. Phys. Chem. 82 (1978) 1801.
[35] N.S. McIntyre, D.G. Zetaruk, D. Owen, J. Electrochem. Soc. 126 (1979) 750.
[36] D. Briggs, M.P. Seah, Practical Surface Analysis: Auger and X-Ray Photoelectron Spectroscopy, John Wiley & Sons, New York, 1996.